Lattice study of the electromagnetic conductivity of the quark-gluon plasma in an external magnetic field

Nikita Astrakhantsev,[1,2,†] V. V. Braguta,[3,4,5,‡] Massimo D'Elia,[6,7,§] A. Yu. Kotov,[3,4,5,*] A. A. Nikolaev,[8,‖] and Francesco Sanfilippo[9,¶]

[1]*Physik-Institut, Universität Zürich, Winterthurerstrasse 190, CH-8057 Zürich, Switzerland*
[2]*Institute for Theoretical and Experimental Physics NRC "Kurchatov Institute", Moscow, 117218 Russia*
[3]*National University of Science and Technology MISIS, Leninsky Prospect 4, Moscow, 119049 Russia*
[4]*Bogoliubov Laboratory of Theoretical Physics, Joint Institute for Nuclear Research, Dubna, 141980 Russia*
[5]*Moscow Institute of Physics and Technology, Institutsky lane 9, Dolgoprudny, Moscow region, 141700 Russia*
[6]*Dipartimento di Fisica dell'Università di Pisa, Largo B. Pontecorvo 3, I-56127 Pisa, Italy*
[7]*INFN, Sezione di Pisa, Largo B. Pontecorvo 3, I-56127 Pisa, Italy*
[8]*Department of Physics, College of Science, Swansea University, Swansea SA2 8PP, United Kingdom*
[9]*INFN, Sezione di Roma Tre, Via della Vasca Navale 84, I-00146 Rome, Italy*

(Received 3 November 2019; revised 28 February 2020; accepted 26 August 2020; published 28 September 2020)

We study the electromagnetic conductivity of QGP in a magnetic background by lattice simulations with $N_f = 2 + 1$ dynamical rooted 2-stout smeared staggered fermions at the physical point. We study the correlation functions of the electromagnetic currents at $T = 200$, 250 MeV and use the Tikhonov approach to extract the conductivity. The conductivity is found to rise with the magnetic field in the parallel direction and to decrease in the transverse direction, giving evidence for both the chiral magnetic effect and the magnetoresistance phenomenon in QGP. We also estimate the chiral charge relaxation time in QGP.

DOI: 10.1103/PhysRevD.102.054516

I. INTRODUCTION

The chiral magnetic effect (CME) is a well known anomaly-based phenomenon which can be realized in different systems with relativistic fermionic degrees of freedom [1–3]. The CME is the generation of a nondissipative electric current along the external magnetic field in systems with a net imbalance between the number of right-handed and left-handed fermions, or nonzero chiral density.

A nonzero chiral density is generally needed in order to experimentally observe the CME. In heavy-ion experiments such density might be generated due to sphaleron transitions in the quark-gluon plasma (QGP) [4,5]. In condensed matter systems the chiral density can be generated as the result of lattice deformations [6]. Another way to generate the chiral density and to observe the CME is to apply parallel electric and magnetic fields; in this case the chiral anomaly generates the imbalance between the right-handed and left-handed fermions which leads to the CME manifesting itself through the rise of electric conductivity along the magnetic field. This CME current has already been observed experimentally in condensed matter systems [7–9].

Similarly to condensed matter systems, the latter mechanism can be realized in heavy-ion experiments, where colliding ions create hot QGP with deconfined relativistic quarks. In addition, in noncentral collisions the QGP is affected by huge magnetic fields generated by the motion of colliding heavy ions [4]. As a result the electromagnetic conductivity of QGP along the magnetic field might be significantly enhanced.

Let us consider QGP in parallel electric $\mathbf{E}$ and magnetic $\mathbf{B}$ fields. Due to the axial anomaly these fields lead to the generation of a chiral density with the rate [7]

$$\frac{d\rho_5}{dt} = C\frac{e^2}{2\pi^2}\mathbf{E}\cdot\mathbf{B} - \frac{\rho_5}{\tau}, \tag{1}$$

where $C = N_c \sum_f q_f^2$. The first term in Eq. (1) describes the production of chiral charge due to the chiral anomaly,

*Corresponding author.
andrey.kotov@phystech.edu
†nikita.astrakhantsev@physik.uzh.ch
‡braguta@itep.ru
§massimo.delia@unipi.it
‖aleksandr.nikolaev@swansea.ac.uk
¶francesco.sanfilippo@roma3.infn.it

while the second term stands for the decrease of chirality due to chirality-changing processes with the relaxation time τ. Note that Eq. (1) has the stationary solution

$$\rho_5 = C\frac{e^2}{2\pi^2}\mathbf{E}\cdot\mathbf{B}\tau, \tag{2}$$

which describes the balance between anomaly based production rate and chirality relaxation processes.

The chiral charge density can be parametrized by the chiral chemical potential μ_5 through the equation of state $\rho_5 = \rho_5(\mu_5)$. We use the linear response theory and consider the electric field $\mathbf{E}$ as a perturbation. In this limit the generated chiral chemical potential is small and the equation of state reads $\rho_5 = \mu_5\chi(T,B) + O(\mu_5^3)$, where the $\chi(T,B)$ is a function of magnetic field and temperature. We mainly consider large magnetic fields ($q_f eB \gg T^2$), thus the chiral density is governed by the lowest Landau level degeneracy, $\chi \propto eB$ ($\chi = N_c\sum_f |q_f|eB/2\pi^2$ in the non-interacting approximation). The CME generates the electric current

$$\mathbf{j}_{\mathrm{CME}} = C\frac{e^2}{2\pi^2}\mu_5\mathbf{B}. \tag{3}$$

Combining Eq. (2) and Eq. (3) one obtains the conductivity due to the CME

$$j^i_{\mathrm{CME}} = \sigma^{ij}_{\mathrm{CME}}E^j, \qquad \sigma^{ij}_{\mathrm{CME}} = C^2\frac{e^4}{4\pi^4}\frac{\tau}{\chi(T,B)}B^iB^j, \tag{4}$$

it is assumed here that the magnetic field is applied along the z axis.

In addition to the CME current there is also Ohmic current in the system and the total conductivity reads $\sigma = \sigma^O + \sigma^{\mathrm{CME}}$. If the electric field is applied along the x axis, the Lorentz force reduces the transverse conductivity σ^O_{xx}. The $\sigma^{\mathrm{CME}}_{xx}$ component is zero in this case. The decrease of σ_{xx} in an external magnetic field is called magnetoresistance. On the other hand, if an electric field is applied along the magnetic field, there is no Lorentz force and magnetoresistance. At the same time $\sigma^{\mathrm{CME}}_{zz}$ is a rising function of the magnetic field, and this can be a manifestation of the CME.[1] Thus the transport properties of QGP in can be considerably modified by the external magnetic field.

It should be noted that the electromagnetic conductivity of QCD was calculated in a number of lattice studies (see for instance [10–13]). At the same time, some electromagnetic properties of the QGP in the presence of a magnetic background, like its magnetic susceptibility, have been already explored [14–21], as well as the emergence of anisotropies related to the magnetic background in other relevant quantities [17,22–26]. A quenched lattice study of the electromagnetic conductivity of QCD in external magnetic field was carried out in [27], where no sign of either CME or magnetoresistance in QGP was found. We would like to mention also the lattice study of the electromagnetic conductivity in the presence of external magnetic fields in Dirac semimetals [28], where both CME and magnetoresistance were observed in the semimetal phase, which is similar to the QGP phase in some properties. The conductivity of QGP in external magnetic fields was also studied within holographic models [29] and by means of kinetic theory [30,31]. Finally we would like to mention lattice study of the CME in thermodynamic equilibrium [32].

This paper is organized as follows. In the next section we discuss technical details of our lattice study. In Sec. III we describe the Backus-Gilbert and Tikhonov regularization methods used to extract the conductivity from Euclidean correlation functions. Numerical results are presented in the Sec. IV. Finally, in the last section, we discuss our results and draw our conclusions.

II. THE LATTICE SETUP

We simulate $2+1$ flavors QCD using 2-stout improved rooted staggered fermions and the tree-level Symanzik improved gauge action [33,34]. The partition function can be written as

$$Z(B) = \int \mathcal{D}U e^{-S_{\mathrm{YM}}}\prod_{f=u,d,s}\det(D^f_{\mathrm{st}}[B])^{1/4}, \tag{5}$$

where

$$S_{\mathrm{YM}} = -\frac{\beta}{3}\sum_{i,\mu\neq\nu}\left(\frac{5}{6}P^{1\times1}_{i;\mu\nu} - \frac{1}{12}P^{1\times2}_{i;\mu\nu}\right), \tag{6}$$

and the symbols $P^{1\times1}_{i;\mu\nu}$ and $P^{1\times2}_{i;\mu\nu}$ denote the real part of the trace of 1×1 and 1×2 loops. The staggered matrix is

$$(D^f_{\mathrm{st}})_{i,j} = am_f\delta_{i,j} + \sum_{\nu=1}^{4}\frac{\eta_{i;\nu}}{2}\left(u^f_{i;\nu}U^{(2)}_{i;\nu}\delta_{i,j-\hat{\nu}} - u^{f*}_{i-\hat{\nu};\nu}U^{(2)\dagger}_{i-\hat{\nu};\nu}\delta_{i,j+\hat{\nu}}\right), \tag{7}$$

where $\eta_{i;\nu}$ are the staggered phases, $U^{(2)}_{i;\mu}$ stands for the two times stout-smeared link [35] (with isotropic smearing parameter $\rho = 0.15$) and $u^f_{i;\mu}$ is the Abelian field phase.

The Abelian transporters corresponding to a uniform magnetic field B_z directed along $\hat{z}$ can be chosen as

[1] In what follows the transverse conductivity σ_{xx} will be designated as $\sigma_\perp$, while the conductivity along magnetic field σ_{zz} will be designated as $\sigma_\parallel$.

$$u^f_{i;y} = e^{ia^2 q_f B_z i_x}, \qquad u^f_{i;x}|_{i_x=N_x} = e^{-ia^2 q_f N_x B_z i_y}, \quad (8)$$

where q_f is the quark charge and all the other Abelian links are set to 1 (N_k is the lattice extent in the $\hat{k}$ direction, $1 \le i_k \le N_k$). B_z cannot be arbitrary: for Eq. (8) to describe a uniform magnetic field on a lattice torus, the value B_z must be quantized as follows [36–38]

$$\frac{e}{3} B_z = 2\pi b/(a^2 N_x N_y), \quad (9)$$

where b is an integer.

We consider two values of temperature $T = 200, 250$ MeV; most simulations are carried out on a 16×64^3 lattice, with spacings $a = 0.0618$ fm and $a = 0.0493$ fm correspondingly. To check the lattice spacing dependence we also consider a 10×48^3 lattice with $a = 0.0988$ fm. To study the ultraviolet (UV) properties of the correlator of two electromagnetic currents we perform simulations on a 96×48^3 lattice at $a = 0.0988$ fm, which corresponds to $T \approx 0$.

Bare parameters have been chosen so as to stay on a line of constant physics with physical quark masses. In particular, we adopted the values reported in [39–41], either directly or by interpolation. $O(100)$ decorrelated gauge configurations have been used for each simulation point. Gauge configurations have been sampled using the Rational Hybrid Monte-Carlo algorithm [42–44]. In Table I we report the lattice parameters used in the simulations.

The process of conductivity measurements consists of two parts: correlation function measurement and spectral function extraction via the Kubo formula inversion. The correlation function reads

$$C_{ij}(\tau) = \frac{1}{L_s^3} \langle J_i(\tau) J_j(0) \rangle, \quad (10)$$

where τ is the Euclidean time and $J_i(\tau)$ is the conserved current

$$J_i(\tau) = \frac{1}{4} e \sum_f q_f \sum_{\vec{x}} \eta_i(x) (\bar{\chi}^f_x u^f_{x;i} U^{(2)}_{x,i} \chi^f_{x+i} + \bar{\chi}^f_{x+i} u^{f*}_{x;i} U^{(2)\dagger}_{x,i} \chi^f_x), \quad (11)$$

where $x = (\tau, \vec{x})$, $\eta_i(x) = (-1)^{x_1 + .. x_{i-1}}$, $i = 1, 2, 3$, $\bar{\chi}^f_x$, χ^f_x are staggered fermion fields of $f = u, d, s$ flavors, $U^{(2)}_{x,i}$ is the (stout smeared) gauge field matrix and $u^f_{x;i} U^{(2)}$ is the electromagnetic field phase.

The staggered fermion correlator (10) corresponds to two different operators for the even $\tau = 2n \times a$ and odd $\tau = (2n+1) \times a$ slices. In the continuum limit $C_{ij}(\tau)$ reads

$$C^{\mathrm{e,o}}_{ij}(\tau) = \sum_{\vec{x}} (\langle A_i(x) A_j(0) \rangle - s^{\mathrm{e,o}} \langle B_i(x) B_j(0) \rangle), \quad (12)$$

where $s^{\mathrm{e,o}} = (-1)^\tau$ is the time slice parity and

$$A_i = e \sum_f q_f \bar{\psi}^f \gamma_i \psi^f, \qquad B_i = e \sum_f q_f \bar{\psi}^f \gamma_5 \gamma_4 \gamma_i \psi^f,$$

and ψ^f is Dirac spinor of the flavor f. Notice that the operator A_i corresponds to electromagnetic current in the continuum whereas we would like to remove the B_i contribution.

Next let us recall that the current-current Euclidean correlators both for even and odd slices $C^{\mathrm{e,o}}_{ij}$ are related to its spectral functions $\rho^{\mathrm{e,o}}_{ij}(\omega)$ as

$$C^{\mathrm{e,o}}_{ij}(\tau) = \int_0^\infty \frac{d\omega}{\pi} K(\tau, \omega) \rho^{\mathrm{e,o}}_{ij}(\omega), \quad (13)$$

where $K(\tau, \omega) = \frac{\cosh \omega(\tau - \beta/2)}{\sinh \omega\beta/2}$. The electromagnetic conductivity σ_{ij} is related to the spectral densities $\rho^{\mathrm{e,o}}_{ij}(\omega)$ through the Kubo formulas

$$\frac{\sigma_{ij}}{T} = \frac{1}{2T} \lim_{\omega \to 0} \frac{1}{\omega} (\rho^{\mathrm{e}}_{ij}(\omega) + \rho^{\mathrm{o}}_{ij}(\omega)). \quad (14)$$

The contribution of the correlator $\langle B_i(\tau) B_j(0) \rangle$ to the sum $\rho^e_{ij} + \rho^o_{ij}$ cancels out and in the continuum limit the electromagnetic conductivity is reproduced. Similarly to [10–13,27] in this calculation of the correlation function (10) only connected diagrams are taken into account.

III. THE EXTRACTION OF THE ELECTROMAGNETIC CONDUCTIVITY FROM EUCLIDEAN CORRELATION FUNCTIONS

A. The Backus-Gilbert and Tikhonov regularization methods

Given the correlation functions $C^{\mathrm{e,o}}_{ij}(\tau)$ one needs to invert the integral equation (13) and determine spectral

TABLE I. Parameters used in our numerical simulations.

a, fm	L_s	N_t	T, MeV	$m_l a$	$m_s a$	eB, GeV^2
0.988	48	96	$\simeq 0$	0.0014	0.0394	0.0, 0.53
0.0988	48	10	200	0.0014	0.0394	0.0, 0.53, 0.80, 1.13
0.0618	64	16	200	0.000861	0.02423	0.0, 0.28, 0.51, 0.75, 1.12, 1.49
0.0493	64	16	250	0.000688	0.01937	0.0, 0.73, 1.17, 1.76, 2.35

functions $\rho_{ij}^{\mathrm{e,o}}(\omega)$ to find the conductivity. The maximum entropy method (MEM) is a popular method for the reconstruction of the spectral functions [45], and it was applied for the computation of the electromagnetic conductivity in Refs. [11,27]. However, it is rather difficult to carry out our study with MEM: this is because for staggered fermions we have $N_t/2 = 8$ points (due to the symmetry of the correlator around the point $t = N_t/2$) in the temporal direction, which are split into 4 points for even time slices and 4 points for odd time slices. To conduct the reconstruction in this case, one has to reconstruct separately even and odd spectral functions: we believe that for MEM this is a very complicated task; notice also that MEM can be applied only for positive spectral functions, however this is not the case for the odd branch of the spectral function in a magnetic field. For these reasons, we decided to apply Backus-Gilbert (BG) [46] and Tikhonov regularization (TR) [47] methods.

The BG and TR methods are nonparametric linear approaches which can be used to study the spectral function.[2] These methods are aimed at the solution of the equation

$$C(\tau) = \int_0^{+\infty} \frac{d\omega}{2\pi} \frac{\rho(\omega)}{f(\omega)} K(\omega, \tau), \tag{15}$$

where $K(\omega,\tau) = \frac{\cosh\omega(\tau-\beta/2)}{\sinh\omega\beta/2} f(\omega)$ and $f(\omega)$ is an arbitrary function. In linear methods (including the BG and TR), one reconstructs the estimator $\bar{\rho}(\bar{\omega})$ of the spectral function:

$$\bar{\rho}(\bar{\omega}) = f(\bar{\omega}) \sum_i q_i(\bar{\omega}) C(\tau_i), \tag{16}$$

where $q_i(\bar{\omega})$ are some functions, which exact view will be discussed later. Combining Eq. (15) and (16), one gets the following relation between the estimator $\bar{\rho}(\bar{\omega})$ and the spectral function $\rho(\omega)$:

$$\bar{\rho}(\bar{\omega}) = f(\bar{\omega}) \int_0^{\infty} d\omega \delta(\bar{\omega}, \omega) \frac{\rho(\omega)}{f(\omega)}, \tag{17}$$

where $\delta(\bar{\omega}, \omega)$ is given by the formula:

$$\delta(\bar{\omega}, \omega) = \sum_i q_i(\bar{\omega}) K(x_i, \omega). \tag{18}$$

If the resolution function has a sharp peak around $\bar{\omega}$ and normalized to 1, according to Eq. (17) the estimator $\bar{\rho}(\bar{\omega})$ is a very good approximation to the spectral function $\rho(\omega)$. E.g., if $\delta(\omega, \bar{\omega}) = \delta(\omega - \bar{\omega})$ the estimator of the spectral function would exactly reproduce the spectral function $\tilde{\rho}(\bar{\omega}) = \rho(\bar{\omega})$. In real calculation the resolution function has a peak of finite width of few T, thus the estimator $\bar{\rho}(\bar{\omega})$ averages the spectral function over the region of several T. In particular, in the BG and TR methods (see below) at $\bar{\omega} = 0$ the width of the resolution function is $\sim(3.5\text{–}4)T$.

Now let us discuss, how one should select functions $q_i(\bar{\omega})$ in Eq. (16). One of the reasonable ways is to require the minimization of the width of $\delta(\bar{\omega}, \omega)$. However, it turns out that in this simple case the method becomes unstable and susceptible to noise in the data. Thus, the method requires regularization that should be properly adjusted. The difference between BG and TR methods lies in different ways of this regularization.

Within the BG method one minimizes the functional $\mathcal{H}(\rho(\omega)) = \lambda\mathcal{A}(\rho(\omega)) + (1-\lambda)\mathcal{B}(\rho(\omega))$. The term $\mathcal{A}$ represents the width of the resolution function: $\mathcal{A} = \int_0^{\infty} d\omega \delta(\bar{\omega}, \omega)(\omega - \bar{\omega})^2$. The term $\mathcal{B}(\rho(\omega)) = \mathrm{Var}[\rho(\omega)]$ regularizes $\rho(\omega)$ making it less susceptible to noise. In terms of the covariance matrix and functions $q_i(\bar{\omega})$ used to define $\bar{\rho}(\bar{\omega})$ in Eq. (16), it reads $\mathcal{B}(\vec{q}) = \vec{q}^T \hat{S} \vec{q}$. Thus, statistical uncertainties are reduced at cost of increasing the width of the resolution function through decrease of λ.

The minimization of $\mathcal{H}$ gives the following linear functions on the form (16)

$$q_i(\omega) = \frac{\sum_j W_{ij}^{-1}(\bar{\omega}) R(x_j)}{\sum_{kj} R(x_k) W_{kj}^{-1}(\bar{\omega}) R(x_j)}, \tag{19}$$

$$W_{ij}(\bar{\omega}) = \lambda \int_0^{\infty} d\omega K(x_i, \omega)(\omega - \bar{\omega})^2 K(x_j, \omega) + (1-\lambda) S_{ij}, \tag{20}$$

$$R(x_i) = \int_0^{\infty} d\omega K(x_i, \omega). \tag{21}$$

The TR method is another way of the regularization of the same problem. While in the BG method the regularization is performed as $W_{ij} \to \lambda S_{ij} + (1-\lambda) W_{ij}$, in the TR scheme the SVD decomposition of $W^{-1} = VDU^T$ is regularized. The diagonal matrix $D = \mathrm{diag}(\sigma_1^{-1}, \sigma_2^{-1}, \ldots, \sigma_n^{-1})$ might have very large entries that represent the susceptibility of the data to noise. The regularization is done by adding the regularizer γ to all entries as $\tilde{D} = \mathrm{diag}((\sigma_1 + \gamma)^{-1}, (\sigma_2 + \gamma)^{-1}, \ldots, (\sigma_n + \gamma)^{-1})$. Thus, small σ_i will be smoothly cutoff.

In Fig. 1 we plot typical resolution functions for BG and TR regularizations at different $\bar{\omega}$ for the $\lambda = 0.01$ and $\gamma = 1$.

We would like to note that the TR and BG methods can reliably reconstruct $\rho(\omega = 0)$ if the resolution function $\delta(\bar{\omega} = 0, \omega)$ is narrower than the characteristic variation scale of $\rho(\omega)$. Correlation functions of the electromagnetic currents are well described by either the ansatz combining the transport peak at small frequencies and UV contribution at large frequencies [11–13] or by the AdS/CFT spectral

[2]The BG and TR methods were used to study transport properties of different strongly correlated systems in [12,48–50].

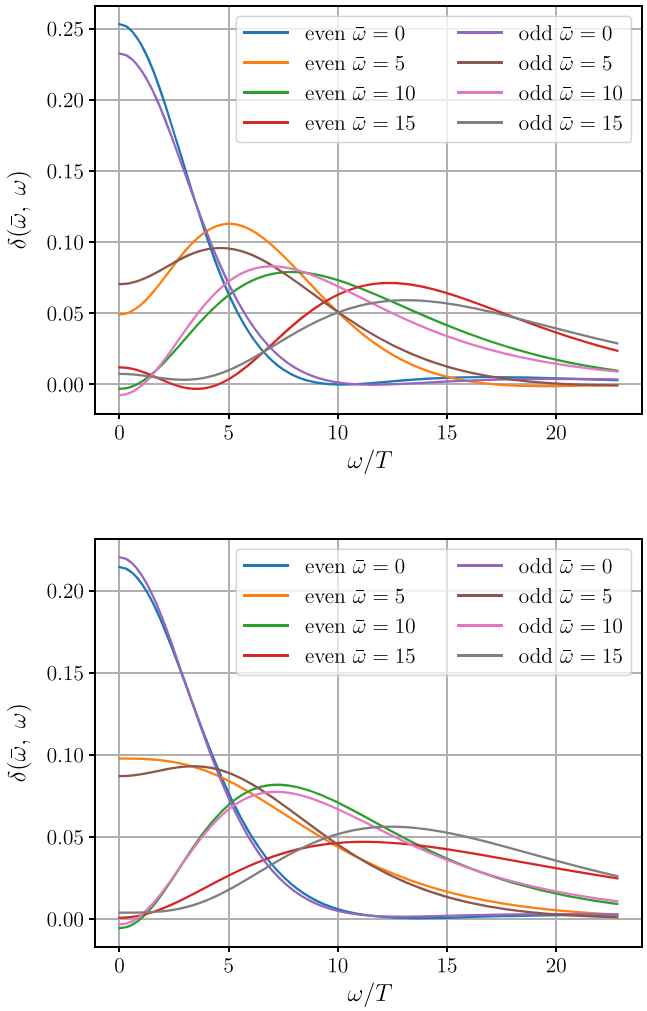

FIG. 1. Top: the resolution functions for the BG regularization at $T = 200$ MeV and $\lambda = 0.01$. Bottom: the resolution functions for the TR regularization at $T = 200$ MeV and $\gamma = 1.0$.

function [13]. Within the temperature interval considered in this paper the widths of $\delta(\bar{\omega} = 0, \omega)$ are close to or smaller than the variation scale of $\rho(\omega)$ obtained in [11–13]. For this reason we believe that both approaches give reliable results for the conductivity extracted from such spectral functions.

One might also expect that slightly above T_c there is a contribution of the ρ–meson remnants that might lead to a slight contamination of our results. However, the most recent lattice studies of the electromagnetic conductivity and the corresponding spectral function [11–13] did not find a sign of the ρ-meson contribution to the spectral function in the temperature range under consideration in our paper. One should also note that our results obtained at zero magnetic field are in agreement with that obtained in previous lattice studies [10,12] (see Fig. 5), within present uncertainties. So, even if there is some contamination of our results due to the remnant of the ρ-meson, it is within the uncertainty of the calculation. Finally, notice that the main focus of the paper is not the electromagnetic conductivity itself, but the change of the conductivity due to nonzero external magnetic field. Consequently, we calculate the difference $\sigma(eB) - \sigma(eB = 0)$ instead of the conductivity $\sigma(eB)$. This further reduces the possible ρ–meson contamination of our results in the deconfinement phase, since one can expect that this contribution will be mostly canceled out in the difference $\sigma(eB) - \sigma(eB = 0)$.

We remark that both in the BG and TR methods, the resolution function is an outcome of the method itself, and cannot be chosen *a priori*. This makes it difficult to well define a continuum limit, since there is no guarantee that the measured quantity is defined in the same way across different gauge ensemble. However, in our calculation we empirically observe that the dependence of the resolution functions on the parameters of the calculation is very weak. This is reflected in the good agreement of the results of $N_t = 10$ and $N_t = 16$ lattices. In the future, if a continuum limit has to be carried out, a fixed resolution function must be employed, for example following the approach suggested in [51].

Our calculation shows that both the BG and TR methods give similar results of the conductivity but the TR resolution function for the conductivity is a little narrower. For this reason in what follows we use the TR approach to calculate the electromagnetic conductivity.

B. The calculation of the electromagnetic conductivity at zero magnetic field $eB = 0$

The calculation of the electromagnetic conductivity is carried out in the following steps. Firstly, we measure the lattice correlation functions $C_{ij}^{\mathrm{e,o}}(\tau)$ (12). Then we calculate the estimators $\tilde{\rho}^{\mathrm{e,o}}(\bar{\omega})/\bar{\omega}$ at $\bar{\omega} = 0$ within the TR approach. Finally using Eq. (14) we calculate the electromagnetic conductivity.

An important issue in the calculation is the UV contribution to the reconstructed conductivity. For instance, in the studies of shear and bulk viscosities of gluon plasma [48,49] the UV spectral density scales as $\rho \propto \omega^4$, which results in a large UV contribution to the estimator. This contribution should be subtracted in order to obtain reliable results. For the conductivity the UV contribution scales as $\rho \propto \omega^2$ and our calculation shows that the UV gives ~20–30% contribution at $\bar{\omega} = 0$.

For zero magnetic field we subtract the ultraviolet contributions from even and odd spectral densities separately. To this end, we employ the model for the spectral densities at large frequencies. Taking into account asymptotic freedom in QCD it is reasonable to assume that real spectral densities at $\omega \gg \Lambda_{\mathrm{QCD}}$ do not deviate considerably from their tree level expressions. This assumption will be confirmed below. It allows us to propose the following forms of the spectral densities at large frequencies

$$\rho^{\mathrm{e,o}}_{\mathrm{UV}}(\omega) = Z_{\mathrm{e,o}} \frac{3}{4\pi^2}\omega^2 \tanh\left(\frac{\omega\beta}{4}\right), \tag{22}$$

where Z_{e}, Z_{o} are the coefficients for the even and odd branches. At the tree level approximation $Z_{\mathrm{e}} = \frac{1}{2}$, $Z_{\mathrm{o}} = \frac{3}{2}$, but these coefficients can be renormalized by the interactions.

In [49,52] it was shown that the BG method with proper scaling can be used to determine the UV coefficient such as Z_{e}, Z_{o}. Following [49,52], we apply BG approach with the rescaling function[3] $f(\omega) = \frac{3}{4\pi^2}\omega^2 \tanh(\frac{\omega\beta}{4})$ and use the lattice data for the correlators calculated on the lattice 96×48^3.

In Fig. 2 we plot the UV behavior of the rescaled reconstructed spectral function $\tilde{\rho}(\bar{\omega})$ for different values of $\lambda = 10^{-4}, 10^{-5}, 10^{-6}$ at the tree level case. From Fig. 2 one can see that the reconstructed asymptotic values match the tree-level values $3/2$, $1/2$, what confirms the validity of the method.

In Fig. 3 we perform the same procedure in the interacting case for $\lambda = 10^{-4}, 10^{-5}, 10^{-6}$. From Fig. 3 it is seen that in the UV the spectral functions indeed correspond to the models (22). Notice also that the coefficients Z_{e}, Z_{o} are considerably renormalized as compared to their tree level values, but their mean value is only slightly renormalized, $A = (Z_{\mathrm{e}} + Z_{\mathrm{o}})/2 \sim 1.0$. Taking into account the uncertainties of the calculation we obtain $A = 1.05 \pm 0.05$. Note that this result agrees with previous calculations [12,13], where the renormalization of A was shown to be small.

Finally, to perform the subtraction of the UV contribution, we take the mean value of two branches conductivity $\rho(\omega) = (\rho^e(\omega) + \rho^o(\omega))/2$. Then the UV contribution is subtracted in the form

$$\Delta\tilde{\rho}(\bar{\omega}) = A \int_{\omega_0}^{+\infty} d\omega \delta(\bar{\omega}, \omega) \frac{3}{4\pi^2}\omega^2 \tanh\left(\frac{\omega\beta}{4}\right), \tag{23}$$

where the ω_0 is the frequency which represents the asymptotic freedom region (23) onset. Unfortunately it is not possible to determine the value of ω_0 within the BG method. In the calculation of the conductivity we vary $\omega_0 \in (1.5\ \mathrm{GeV}, 3.0\ \mathrm{GeV})$ and account this as the systematic uncertainty. Note that this range of ω_0 variation is in good agreement with the one obtained in [12] within the fitting procedure.

The uncertainties of conductivity at zero magnetic field come from several sources. The first part of uncertainty is a statistical one, which can be estimated within the Backus-Gilbert method. Note that statistical uncertainty depends on the specific choice of λ regularization. In turn, we estimate

[3]Notice that in order to account discretization uncertainties we use lattice expressions for the function $f(\omega)$.

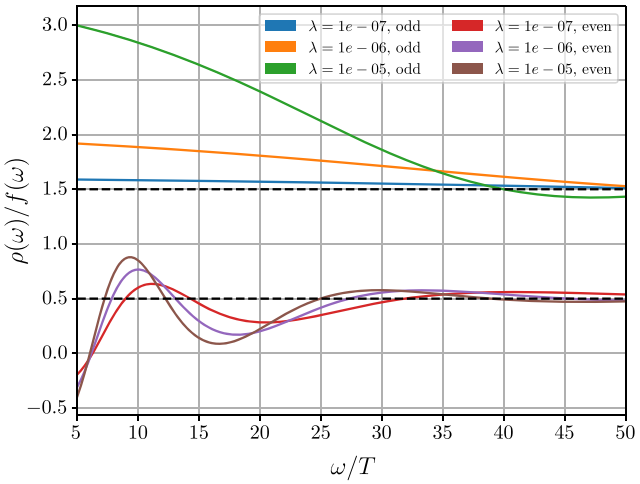

FIG. 2. The reconstructed ultraviolet behavior for odd and even branches of the spectral function on the lattice 96×48^3 at the tree-level approximation and $f(\omega) = \frac{3}{4\pi^2}\omega^2 \tanh(\frac{\omega\beta}{4})$. The reconstruction is carried out for the following values of the $\lambda = 10^{-5}, 10^{-6}, 10^{-7}$. The dashed lines correspond to tree level results $Z_{\mathrm{e}} = \frac{1}{2}$, $Z_{\mathrm{o}} = \frac{3}{2}$.

systematic uncertainty as emerging from two sources: ultraviolet parameters for ultraviolet contamination subtraction and the choice of λ regularizer. The uncertainties on the ultraviolet parameters A (amplitude) and ω_0 (UV cutoff) together result in relative systematic error of ~10–15%, while, surprisingly, the conductivity $\sigma(0)$ is practically insensitive to choice of λ. To account for the uncertainty of λ, in the calculation we take statistical uncertainty to be the largest one while λ is varied within the region [0.1, 10]. This results in relative statistical error of 3%–5%.

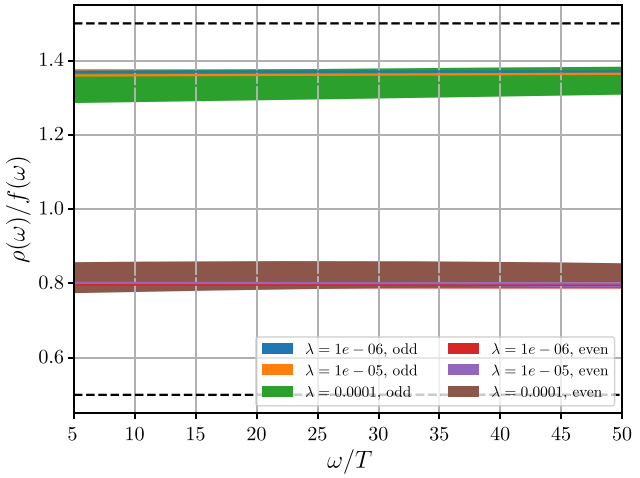

FIG. 3. The reconstructed ultraviolet behavior for odd and even branches of the spectral function on the lattice 96×48^3 in the interacting case and $f(\omega) = \frac{3}{4\pi^2}\omega^2 \tanh(\frac{\omega\beta}{4})$. The reconstruction is carried out for the following values of the $\lambda = 10^{-5}, 10^{-6}, 10^{-7}$. The dashed lines correspond to tree-level results $Z_{\mathrm{e}} = \frac{1}{2}$, $Z_{\mathrm{o}} = \frac{3}{2}$.

C. The calculation of the effects of the magnetic field on the electromagnetic conductivity

Let us now consider the electromagnetic conductivity of QGP in the presence of the external magnetic field. From a technical point of view, the magnetic field affects directly the path-integral measure and the fermion propagators entering the construction of the electromagnetic currents; moreover, the e.m. $U(1)$ phases enter the gauge links in the definition of the split current in Eq. (11). Apart from this, the problem turns out to be easier than at $eB = 0$. In particular, instead of the correlation functions $C^{e,o}_{eB}$ we consider the difference $\Delta C^{e,o} = C^{e,o}_{eB} - C^{e,o}_{eB=0}$. Since, for the chosen values of the lattice spacing, the UV regime starts at $\omega_0 \sim 2$ GeV, we note that $q_f eB \ll \omega^2$ for all frequencies in the UV regime and magnetic fields. Thus, one can consider the UV spectral function magnetic field-independent and assume that the differences $\Delta C^{e,o}$ do not contain the UV contribution. The results for $\Delta C^{e,o}$ turn out to be more accurate since the UV–estimation uncertainty is absent in this case. The correlator $\Delta C^{e,o}$ is related to additional conductivity due to the presence of the magnetic field. In our further study we apply the TR approach to the differences $\Delta C^{e,o}$.

In the reconstruction procedure one has to choose the value of the parameter γ. In order to do this in Fig. 4 we show typical dependence of the ratios $\Delta\sigma_{\parallel}/TC_{\rm em}$ (top panel) and $\Delta\sigma_{\perp}/TC_{\rm em}$ (bottom panel) on the γ parameter and the width Γ_δ of the resolution functions for even and odd branches of the correlator (12); the error bars of the red stars are the statistical uncertainty. Figure 4 is plotted for the lattice 16×64^3 with the parameters $eB = 0.75$ GeV^2 and $T = 200$ MeV. The same figures for the lattices with other parameters studied in this paper look similarly.

From Fig. 4 it is clear that in the region of small γ (weak regularization) the method becomes unstable what manifests itself in large statistical uncertainties rising with the decrease of γ. In addition, in the same region the reconstructed conductivities and the widths of the even and odd resolution functions reach plateaus. Moreover, since the resolution function width does not decrease below some value of γ, the decrease of the γ below this value does not make the reconstruction more accurate.

On the contrary, in the region of large γ the method is stable with small uncertainties at the cost of strong regularization. The widths of the resolution functions are growing and spectral function is averaged over a large region which is not appropriate for the conductivity reconstruction. In order to safely choose the region of regularization uncertainty, we restrict ourselves from below by the value of γ where the plateau is saturated and from above by the value of γ where both resolution functions have the width of $4T$. This results in the variation region roughly $\gamma \in (0.1, 10)$. The exact regions depend on the lattice parameters (magnetic field and temperature).

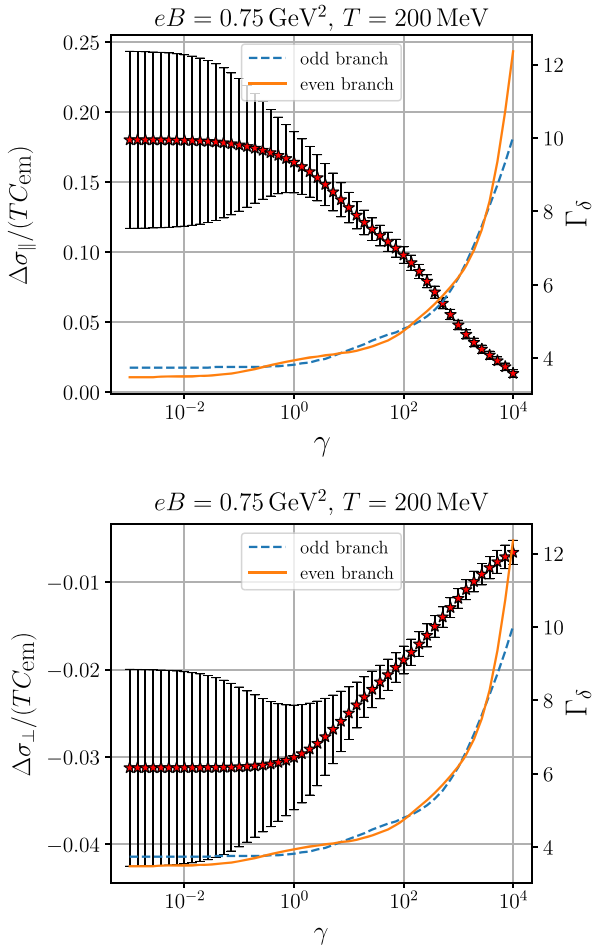

FIG. 4. Left axis: the ratios $\Delta\sigma_{\parallel}/TC_{\rm em}$ (top panel) and $\Delta\sigma_{\perp}/TC_{\rm em}$ (bottom panel) calculated within the Tikhonov regularization procedure (red stars) as a function of the γ parameter for lattice parameters $eB = 0.75$ GeV^2 and $T = 200$ MeV. The error bars of the red stars are due to the statistical uncertainty. Right axis: the width Γ_δ of the resolution function $\delta(\bar{\omega} = 0, \omega)$ as a function of γ for odd (dashed line) and even (solid line) correlation function branches.

Thus, we restrict ourselves to the region $\gamma \in (0.1, 10)$ where the method is stable and the resolution is sufficiently narrow $< 4T$. The uncertainties of our results were estimated as the total variation of the ratio $\Delta\sigma/TC_{\rm em}$ including statistical uncertainties as the γ parameter is varied within the region $\gamma \in (0.1, 10)$.

IV. RESULTS

Let us start with the discussion of results in absence of the external magnetic field. The electromagnetic conductivities normalized to the factor $TC_{\rm em}$ ($C_{\rm em} = e^2 \sum_f q_f^2$) at zero magnetic field and temperatures $T = 200$, 250 MeV are shown in Fig. 5. In addition we plot the results of Refs. [10,12]. Notably our results are in agreement with previous lattice studies within the uncertainties.

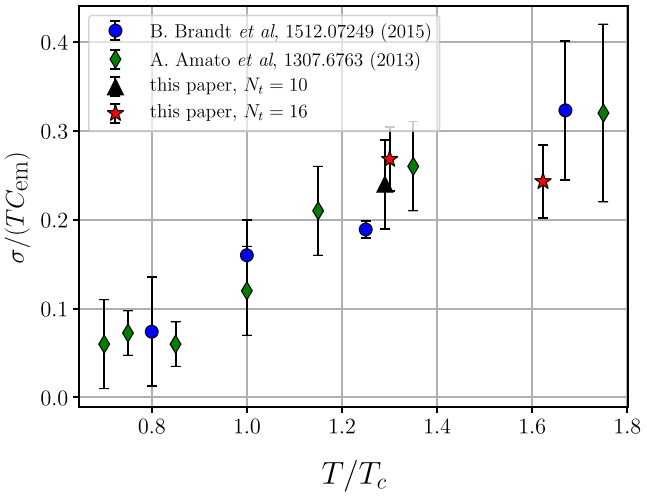

FIG. 5. The electromagnetic conductivity in QCD as a function of temperature normalized to the factor $TC_{\rm em}$ at $eB = 0$. The green rhombi show the $n_f = 2 + 1$ data from [10], the blue circles stand for the $n_f = 2$ data from [12]. The red stars show the results of this study obtained at temperatures $T = 200, 250$ MeV on a 16×64^3 lattice. The black triangle shows the result for $T = 200$ MeV calculated on a 10×48^3 lattice.

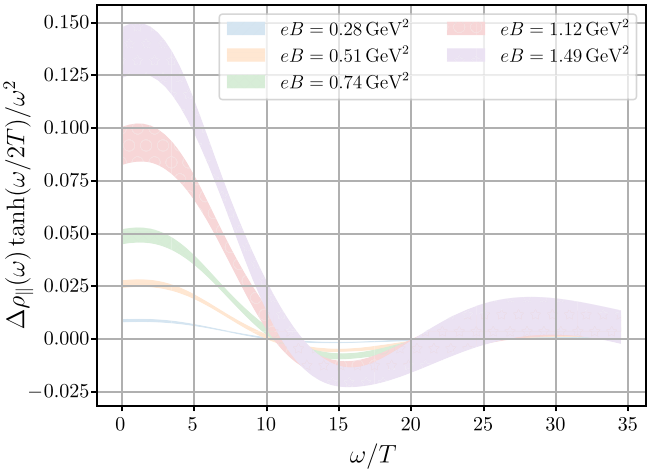

FIG. 6. The reconstructed spectral function $\Delta\rho_\parallel$ from the difference of the correlation functions $\Delta C^{\rm e,o}$ at $T = 200$ MeV for various magnetic fields.

Let us now turn to discussion of the results in presence of external magnetic field. First of all, the emergence of the transport peak can be already observed on the level of the spectral function reconstruction. The reconstructed $\Delta\rho_\parallel(\omega)/f(\omega)$, where $f(\omega) = \omega^2/\tanh\omega/2T$, at $T = 200$ MeV is shown in Fig. 6. It is clear that the infrared part of the spectral function ($\omega/T < 10$) has a transport peak with the height rising with the magnetic field. The UV part of the spectral function weakly depends on the magnetic field and remains close to zero as expected.

Finally, the change of the electromagnetic conductivity due to the external magnetic field $\Delta\sigma = \sigma_{eB} - \sigma_{eB=0}$ normalized to $TC_{\rm em}$ at temperatures $T = 200$, 250 MeV is shown in Fig. 7. It is clear that $\Delta\sigma_\parallel$ rises with the magnetic field, which is an evidence of the presence of CME in QGP; moreover, the rise of $\Delta\sigma_\parallel$ becomes linear for large magnetic fields, in agreement with Eq. (4). A similar linear growth of $\sigma_\parallel$ was obtained in [53] within the kinetic theory. On the contrary, $\Delta\sigma_\perp$ decreases with the magnetic field, which is an evidence of magnetoresistance in QGP. Note also that the slopes of both functions, $\Delta\sigma_\parallel(eB)$ and $\Delta\sigma_\perp(eB)$, decrease with temperature: we believe that this can be explained by a decrease of the relaxation time with temperature because of the increased thermal activity.

In order to estimate the finite N_t effects of we calculate the conductivity at $T = 200$ MeV, $eB = 0, 0.52, 0.79, 1.12$ GeV^2 also on a 10×48^3 lattice, in addition to the 16×64^3 lattice at hand. The results of this calculation are shown in Figs. 5 and 7. It is seen that, within computation uncertainties, the conductivities calculated at different lattice spacings are in agreement with each other.

Is is also instructive to study the independent quark contributions to the CME, since the effect of the magnetic field on the fermion propagators can be separated into u–, d–and s–quark contributions which can be calculated from the quark loop of the corresponding flavor.[4] In Fig. 8 we plot the u–, d–and s–quark contributions to $\Delta\sigma_\parallel(\omega)$, $\Delta\sigma_\perp(\omega)$ normalized to the factor $Te^2q_f^3$ at $T = 250$ MeV. The normalization factor was chosen so as to reduce the dependence of the corresponding contribution on the quark flavor: the q_f^2 results from the correlation function (10) while the additional q_f results from the leading order coupling of the magnetic field to the quark $q_f eH$. From Fig. 8 it is seen that $\Delta\sigma_\perp/q_f^3$ is independent on the quark flavor. In turn, the contributions of the d–and s–quarks to $\Delta\sigma_\parallel/q_f^3$ agree, while the contribution of the u–quark is slightly larger. This can be explained by the larger charge of the u-quark. We thus conclude that the leading dependence of $\Delta\sigma_\parallel$, $\Delta\sigma_\perp$ on the quark flavor is proportional to q_f^3. In addition the relatively heavy s–quark mass does not influence $\Delta\sigma_\parallel(\omega)$ and $\Delta\sigma_\perp(\omega)$.

Finally, the dependence of $\Delta\sigma_\parallel$ on the magnetic field, which is responsible for the CME, allows us to estimate the relaxation time of the chiral charge [see Eq. (4)]. The relaxation times turn out to be $\tau(200\ {\rm MeV}) = 0.26(5)$ fm/c, $\tau(250\ {\rm MeV}) = 0.24(3)$ fm/c, which is in agreement with the relaxation time obtained in [54], where τ lies in the interval ~0.1–1.0 fm/c at $T \sim 200$–250 MeV depending on the model.

[4]Notice that the separation of the conductivity into each flavor contribution is possible only for the connected diagrams.

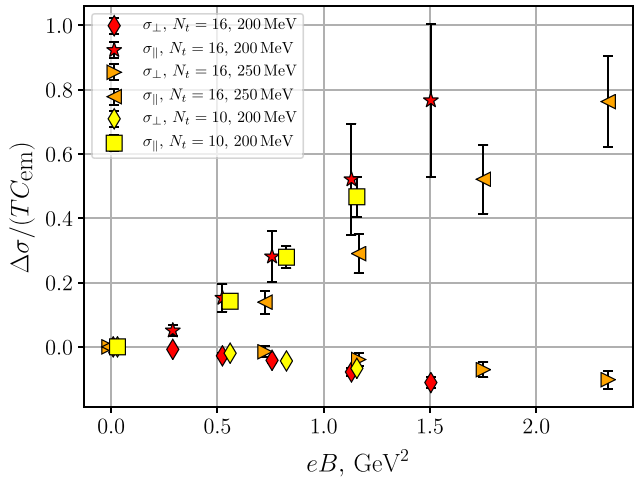

FIG. 7. The electromagnetic conductivities due to the external magnetic field $\Delta\sigma = \sigma_{eB} - \sigma_{eB=0}$ normalized to $TC_{\rm em}$ for $T = 200$, 250 MeV. The $\Delta\sigma_\parallel$, $\Delta\sigma_\perp$ correspond to the directions which are parallel and transverse to the magnetic field. We also show the result for $T = 200$ MeV calculated on the lattice with $N_t = 10$ to check the finite N_t artifacts.

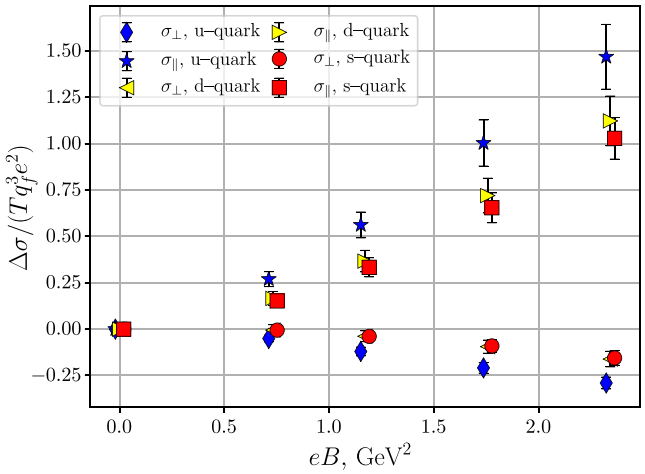

FIG. 8. The u–, d– and s–quark contributions to $\Delta\sigma_\parallel(\omega)$, $\Delta\sigma_\perp(\omega)$ normalized to the factor $Te^2q_f^3$ at $T = 250$ MeV.

V. DISCUSSION AND CONCLUSION

In this paper we studied the electromagnetic conductivity of QGP in a magnetic background by lattice simulations with $N_f = 2 + 1$ dynamical rooted 2-stout smeared staggered fermions at the physical point. We calculated the correlation functions of the electromagnetic currents at $T = 200$, 250 MeV and use the Tikhonov approach to extract the conductivity. It is found that the conductivity along the magnetic field rises with the magnetic field, which is a possible manifestation of the CME. On the contrary, the conductivity in the transverse direction is decreasing with the magnetic field, which is the magnetoresistance phenomenon. Thus we observe evidence for the CME and magnetoresistance in QGP. Finally, we also computed the relaxation time of the chiral charge in QGP for the explored temperature range.

The electromagnetic conductivity of QCD in an external magnetic field was studied in [27] in the quenched approximation, reporting no evidence of either CME or magnetoresistance in QGP. A possible source of the disagreement is the small magnetic field used in [27], where the largest field used in the deconfined phase is $eB = 0.36$ GeV^2: at the same value our signal is quite small (see Fig. 7), so probably the signal was hardly detectable in [27]. The authors of [27] also conducted simulations in the confined phase, observing a rise of $\Delta\sigma_\parallel$ and a drop of $\Delta\sigma_\perp$. Similarly, we have also calculated the conductivities in the confined phase using the approach developed in this paper, obtaining similar results: $\Delta\sigma_\parallel$ rises while $\Delta\sigma_\perp$ drops with the magnetic field.

However, we would like to stress that contrary to the deconfined phase the structure of the spectral function in the confined phase is rather complicated. For instance, it contains the contribution of the intermediate $\pi^+\pi^-$ mesons or the ρ meson peak which has a large spectral weight in the confined phase [12]. It is reasonable to expect that the external magnetic field modifies the spectral function, for instance through the light meson masses modification [55–58]. Thus, in order to check the presence of CME in the confined phase one has to separate the contribution to the spectral function due to the conductivity, $\omega \sim 0$, from the contribution of the light mesons $\omega \sim 2m_\pi, m_\rho, \ldots$. This is a difficult task which can not be done with the data used in this paper; that might be the case for Ref. [27] as well. Note also that in [28] $\Delta\sigma_\parallel$ was studied in Dirac semimetals both in semimetal and insulator phases. Due to chiral symmetry breaking in the insulator phase it was found that $\Delta\sigma_\parallel = 0$ and there is no CME in this phase; in the confined phase there is also chiral symmetry breaking, hence one can expect a similar behavior in this phase as well.

ACKNOWLEDGMENTS

The work of N. A., V. V. B., and A. Yu. K. was supported by RFBR Grants No. 18-02-01107 and No. 18-02-40126. A. A. N. acknowledges the support from STFC via Grant No. ST/P00055X/1. F. S. is supported by the Italian Ministry of Research (MIUR) under Grant No. PRIN 20172LNEEZ and by INFN under No. GRANT73/CALAT. Numerical simulations have been carried out on the MARCONI machine at CINECA, based on the agreement between INFN and CINECA (under Project No. INF19_npqcd), and on the computing resources of the federal collective usage center Complex for Simulation and Data Processing for Mega-science Facilities at NRC "Kurchatov Institute", http://ckp.nrcki.ru/. In addition, the authors used the supercomputer of Joint Institute for Nuclear Research "Govorun".

[1] K. Fukushima, D. E. Kharzeev, and H. J. Warringa, Phys. Rev. D **78**, 074033 (2008).
[2] D. E. Kharzeev, Prog. Part. Nucl. Phys. **75**, 133 (2014).
[3] D. E. Kharzeev, J. Liao, S. A. Voloshin, and G. Wang, Prog. Part. Nucl. Phys. **88**, 1 (2016).
[4] D. E. Kharzeev, L. D. McLerran, and H. J. Warringa, Nucl. Phys. **A803**, 227 (2008).
[5] A. Yu. Kotov, Pis'ma Zh. Eksp. Teor. Fiz. **108**, 374 (2018) [JETP Lett. **108**, 352 (2018)].
[6] A. Cortijo, D. Kharzeev, K. Landsteiner, and M. A. H. Vozmediano, Phys. Rev. B **94**, 241405 (2016).
[7] Q. Li, D. E. Kharzeev, C. Zhang, Y. Huang, I. Pletikosic, A. V. Fedorov, R. D. Zhong, J. A. Schneeloch, G. D. Gu, and T. Valla, Nat. Phys. **12**, 550 (2016).
[8] C.-Z. Li, L.-X. Wang, H. Liu, J. Wang, Z.-M. Liao, and D.-P. Yu, Nat. Commun. **6**, 10137 (2015).
[9] H. Li, H. He, H.-Z. Lu, H. Zhang, H. Liu, R. Ma, Z. Fan, S.-Q. Shen, and J. Wang, Nat. Commun. **7**, 10301 (2016).
[10] A. Amato, G. Aarts, C. Allton, P. Giudice, S. Hands, and J.-I. Skullerud, Phys. Rev. Lett. **111**, 172001 (2013).
[11] G. Aarts, C. Allton, A. Amato, P. Giudice, S. Hands, and J.-I. Skullerud, J. High Energy Phys. 02 (2015) 186.
[12] B. B. Brandt, A. Francis, B. Jger, and H. B. Meyer, Phys. Rev. D **93**, 054510 (2016).
[13] H.-T. Ding, O. Kaczmarek, and F. Meyer, Phys. Rev. D **94**, 034504 (2016).
[14] C. Bonati, M. D'Elia, M. Mariti, F. Negro, and F. Sanfilippo, Phys. Rev. Lett. **111**, 182001 (2013).
[15] L. Levkova and C. DeTar, Phys. Rev. Lett. **112**, 012002 (2014).
[16] C. Bonati, M. D'Elia, M. Mariti, F. Negro, and F. Sanfilippo, Phys. Rev. D **89**, 054506 (2014).
[17] G. S. Bali, F. Bruckmann, G. Endrodi, and A. Schafer, Phys. Rev. Lett. **112**, 042301 (2014).
[18] G. S. Bali, F. Bruckmann, G. Endrődi, S. D. Katz, and A. Schäfer, J. High Energy Phys. 08 (2014) 177.
[19] K. Hattori and D. Satow, Phys. Rev. D **94**, 114032 (2016).
[20] K. Fukushima and Y. Hidaka, J. High Energy Phys. 04 (2020) 162.
[21] V. V. Braguta, M. N. Chernodub, A. Yu. Kotov, A. V. Molochkov, and A. A. Nikolaev, Phys. Rev. D **100**, 114503 (2019).
[22] C. Bonati, M. D'Elia, M. Mariti, M. Mesiti, F. Negro, and F. Sanfilippo, Phys. Rev. D **89**, 114502 (2014).
[23] C. Bonati, M. D'Elia, M. Mariti, M. Mesiti, F. Negro, A. Rucci, and F. Sanfilippo, Phys. Rev. D **94**, 094007 (2016).
[24] C. Bonati, M. D'Elia, M. Mariti, M. Mesiti, F. Negro, A. Rucci, and F. Sanfilippo, Phys. Rev. D **95**, 074515 (2017).
[25] C. Bonati, S. Calí, M. D'Elia, M. Mesiti, F. Negro, A. Rucci, and F. Sanfilippo, Phys. Rev. D **98**, 054501 (2018).
[26] P. Buividovich, M. Polikarpov, and O. Teryaev, Lattice studies of magnetic phenomena in heavy-ion collisions, in *Strongly Interacting Matter in Magnetic Fields*, Lecture Notes in Physics Vol. 871 (Springer, Berlin, Heidelberg, 2013), pp. 377–385.
[27] P. V. Buividovich, M. N. Chernodub, D. E. Kharzeev, T. Kalaydzhyan, E. V. Luschevskaya, and M. I. Polikarpov, Phys. Rev. Lett. **105**, 132001 (2010).
[28] D. L. Boyda, V. V. Braguta, M. I. Katsnelson, and A. Yu. Kotov, Ann. Phys. (Amsterdam) **396**, 78 (2018).
[29] W. Li, S. Lin, and J. Mei, Phys. Rev. D **98**, 114014 (2018).
[30] S. Lin and L. Yang, Phys. Rev. D **101**, 034006 (2020).
[31] L. Thakur and P. K. Srivastava, Phys. Rev. D **100**, 076016 (2019).
[32] A. Yamamoto, Phys. Rev. Lett. **107**, 031601 (2011).
[33] P. Weisz, Nucl. Phys. **B212**, 1 (1983).
[34] G. Curci, P. Menotti, and G. Paffuti, Phys. Lett. **130B**, 205 (1983); **135B**, 516(E) (1984).
[35] C. Morningstar and M. J. Peardon, Phys. Rev. D **69**, 054501 (2004).
[36] G. 't Hooft, Nucl. Phys. **B153**, 141 (1979).
[37] P. H. Damgaard and U. M. Heller, Nucl. Phys. **B309**, 625 (1988).
[38] M. H. Al-Hashimi and U. J. Wiese, Ann. Phys. (Amsterdam) **324**, 343 (2009).
[39] Y. Aoki, S. Borsanyi, S. Durr, Z. Fodor, S. D. Katz, S. Krieg, and K. K. Szabo, J. High Energy Phys. 06 (2009) 088.
[40] S. Borsanyi, G. Endrodi, Z. Fodor, A. Jakovac, S. D. Katz, S. Krieg, C. Ratti, and K. K. Szabo, J. High Energy Phys. 11 (2010) 077.
[41] S. Borsanyi, Z. Fodor, C. Hoelbling, S. D. Katz, S. Krieg, and K. K. Szabo, Phys. Lett. B **730**, 99 (2014).
[42] M. A. Clark, A. D. Kennedy, and Z. Sroczynski, Nucl. Phys. B, Proc. Suppl. **140**, 835 (2005).
[43] M. A. Clark and A. D. Kennedy, Phys. Rev. Lett. **98**, 051601 (2007).
[44] M. A. Clark and A. D. Kennedy, Phys. Rev. D **75**, 011502 (2007).
[45] M. Asakawa, T. Hatsuda, and Y. Nakahara, Prog. Part. Nucl. Phys. **46**, 459 (2001).
[46] G. Backus and F. Gilbert, Geophys. J. Int. **16**, 169 (1968).
[47] A. N. Tikhonov, Sov. Math. Dokl. **4**, 1035 (1963).
[48] N. Astrakhantsev, V. Braguta, and A. Kotov, J. High Energy Phys. 04 (2017) 101.
[49] N. Yu. Astrakhantsev, V. V. Braguta, and A. Yu. Kotov, Phys. Rev. D **98**, 054515 (2018).
[50] D. Boyda, V. Braguta, M. Katsnelson, and M. Ulybyshev, Phys. Rev. B **94**, 085421 (2016).
[51] M. Hansen, A. Lupo, and N. Tantalo, Phys. Rev. D **99**, 094508 (2019).
[52] N. Y. Astrakhantsev, V. Braguta, and A. Y. Kotov, J. High Energy Phys. 04 (2017) 101.
[53] K. Fukushima and Y. Hidaka, Phys. Rev. Lett. **120**, 162301 (2018).
[54] M. Ruggieri, G. X. Peng, and M. Chernodub, Phys. Rev. D **94**, 054011 (2016).
[55] G. S. Bali, B. B. Brandt, G. Endrdi, and B. Glle, Phys. Rev. D **97**, 034505 (2018).
[56] E. V. Luschevskaya, O. E. Solovjeva, and O. V. Teryaev, J. High Energy Phys. 09 (2017) 142.
[57] M. A. Andreichikov, B. O. Kerbikov, E. V. Luschevskaya, Yu. A. Simonov, and O. E. Solovjeva, J. High Energy Phys. 05 (2017) 007.
[58] E. Luschevskaya, O. Teryaev, D. Golubkov, O. Solovjeva, and R. Ishkuvatov, J. High Energy Phys. 11 (2018) 186.